

# Measurement of Viscoelastic Properties of Polyacrylamide-Based Tissue-Mimicking Phantoms for Ultrasound Elastography Applications

Kishore Kumar, *Graduate Student Member, IEEE*, Maneesha E. Andrews, V. Jayashankar, *Member, IEEE*, Ashok K. Mishra, and S. Suresh

**Abstract**—Many ailments and/or malfunctions of the body have been observed to change the viscous behavior and elastic properties of biological soft tissues. The technique of elastography has evolved to image such properties. The clinical evidence gathered during studies involving elastography to identify cancerous lesions is very promising. However, the quantification of the resolution and specificity of elastography is best achieved under a controlled study using tissue-mimicking phantoms. One challenge is to reproduce viscoelastic behavior in phantoms as observed in biological tissues. In this paper, polyacrylamide gel based tissue-mimicking phantoms have been developed to experimentally study the role of viscoelastic properties in a controlled manner. To measure the Young's modulus, the phantoms were subjected to linear loading, and the stress-strain relationship is deduced therefrom. It is seen that the phantoms show hysteresis behavior. The viscoelastic properties of these phantoms were measured by subjecting the samples to cyclic loading. Normal forces during this process of loading were also measured as a measure of sample elasticity. To emulate the normal and pathological lesions, samples were prepared with varying concentration of monomer and studied. Three models, namely, Maxwell, Kelvin-Voigt (KV), and Kelvin-Voigt fractional derivative (KVFD), were chosen to fit the experimental data. Of these, the KVFD model was found to be best fitting for the experimental data obtained. Results indicate that stiffer samples exhibit large variations in the storage modulus when the precompression levels are altered.

**Index Terms**—Elastography, loss modulus, normal force, storage modulus, tissue phantom, viscoelastic.

## I. INTRODUCTION

**I**N CLINICAL practice, manual palpation is often used to diagnose the presence of localized tumors in superficial organs like breast, thyroid, etc. Here, the abnormality is detected by a physician by touching the lesion with finger tips. Data available on the elastic properties of the tissues are limited to blood vessels, skeletal muscle, heart muscle, bone, and cartilage [1], [2]. The mechanical behavior of breast and prostate tissue samples

under compressive loading has been investigated in [3]. Tissue samples were tested at two different precompression levels (5% and 20%) to evaluate the viscoelastic properties of the materials. The results showed that ductal carcinoma and infiltrating ductal carcinomas were much stiffer than any other breast tissues, and these stiffness values were clearly distinguishable at higher levels of precompression applied on the sample. The measurement of mechanical properties using cyclic loading was also reported for other tissue samples such as normal human liver [4], normal and pathological (fibrosis) human liver [5], canine liver [6], veal liver [7], and pig kidney [8]. A method of imaging the mechanical properties of biological tissues using a force-sensitive wheeled probe was proposed [9], and a mechanical image was generated [10] by rolling the wheeled probe across the surface of a solid organ. The validation of the method was carried out on silicon phantoms and excised porcine livers. A summary of viscoelastic properties of various tissues as evident in the literature is presented in Table I.

As opposed to a procedure involving human intervention, there are several techniques that use phase-sensitive imaging modalities such as ultrasound [11]–[13] and magnetic resonance imaging [14], [15] to image the mechanical properties of soft tissues. The basis for the development of these methods is that disease processes alter tissue elastic properties [1], [16]. The measurements of these properties were done using external quasi-static [11] or dynamic [17] excitations or using ultrasound-generated radiation force [18], [19]. Ultrasound elastography is a method to identify pathological changes by measuring elastic properties of tissues [11], [16] using ultrasound. In elastography imaging, the displacement or strain produced inside the lesion due to the application of an external force is measured. The load applied in this method is either static or dynamic. Clinical ultrasound elastography imaging of breast [12], [20] and thyroid [13], [21] has shown promising results in differentiating benign versus malignant lesions on the basis of elastographic contrast. Malignant lesions appear as stiff regions (low strain or high modulus), as compared with the background. Elastic strain images can be nonspecific if the mechanical response depends on the physiological and cellular microenvironmental processes [22] of a specific patient. These changes can be detected by imaging viscoelastic features in combination with elastic features.

A new imaging technique such as elastography needs thorough evaluation in terms of potential limitations in system

Manuscript received June 23, 2009; revised October 12, 2009. Current version published April 7, 2010. The Associate Editor coordinating the review process for this paper was Dr. Salvatore Baglio.

K. Kumar and V. Jayashankar are with the Department of Electrical Engineering, Indian Institute of Technology (IIT) Madras, Chennai 600 036, India (e-mail: jshankar@iitm.ac.in).

M. E. Andrews and A. K. Mishra are with the Department of Chemistry, IIT Madras, Chennai 600 036, India.

S. Suresh is with Mediscan Systems, Chennai 600 004, India.

Color versions of one or more of the figures in this paper are available online at <http://ieeexplore.ieee.org>.

Digital Object Identifier 10.1109/TIM.2009.2038002

TABLE I  
ELASTIC MODULI OF VARIOUS BIOLOGICAL TISSUES  
MEASURED BY APPLYING CYCLIC LOADING

Sample	Elastic modulus	Reference	Comments
Liver Normal Pathological (fibrosis)	2 kPa (15% strain) 20 kPa (15% strain)	Yeh <i>et al</i> [5]	Unconfined compressive method with cyclic loading at three strain conditions – 5%, 10% and 15%
Canine liver	Complex Young's modulus 4 kPa – 9 kPa	Kiss <i>et al</i> [6]	Viscoelastic properties using dynamic mechanical analyzer for frequencies 0.1 Hz – 100 Hz
Veal liver normal Prostate normal	12.9 kPa - 29.9 kPa 18 kPa – 22 kPa	Zhang <i>et al</i> [7]	Crawling wave oscillator (CWE), mechanical measurements
Pig kidney normal	Storage modulus 1 kPa – 10 kPa	Nasseri <i>et al</i> [8]	Rheological tests (shear) – storage and loss modulus for frequencies 0.01 Hz – 100 Hz
Liver normal	2 kPa – 8 kPa	Liu <i>et al</i> [4]	Rheological tests (shear) – storage and loss modulus for frequencies 0.01 Hz – 20 Hz
Breast normal cancerous Prostate Normal cancerous	28 kPa – 66 kPa 93 kPa – 558 kPa 55 kPa – 71 kPa 96 kPa – 241 kPa	Krouskop <i>et al</i> [3]	Precompression (5% and 20%) and cyclic loading with low frequencies 0.1, 1 and 4 Hz

performance [15], [23], [24], accuracy, resolution, and contrast [15], [25], and patient safety to determine its utility in medical diagnosis. The performance evaluation of most of imaging techniques are time consuming. Hence, biological tissues cannot be used as they lose their characteristics with time when harvested away from the human body. In such a context, it becomes necessary to develop tissue-mimicking phantoms that maintain their properties for a long time. Furthermore, a study on phantoms can yield precise information on elastography instrumentation parameters such as gain setting, dynamic range, depth of penetration, center frequency, amount of compressive force to be applied, etc. It is required to have precise knowledge of the amount of deformation undergone by the tissue in response to the stress applied to maximize the visibility of lesions in an elastogram. Phantoms that mimic both acoustic and elastic properties of soft biological tissues aid in establishing a reference standard for elastography image acquisition and, hence, can be used as a tool for a better understanding of the elastographic appearance of different pathological conditions. The imaging of viscoelasticity properties of gelatin hydrogels and breast tissues was attempted in [22]. The measurement techniques used were cyclic loading, creep, and stress relaxation. From the experimental investigations, a concise feature set [26] consisting of elastic strain  $\varepsilon_0$  and retardance times  $T_1$  and  $T_2$  were proposed. The measurement of viscoelastic properties of polyvinyl alcohol phantoms using diffusing wave spectroscopy was presented in [27]. Previous work on the use of polyacrylamide phantoms for ultrasound elastography applications was reported in [28] and [29]. In these studies, the structural properties, including viscoelastic behavior, were not quantified. Other examples of polyacrylamide tissue-mimicking phantoms for ultrasound elastography applications are in [30] and [31]. The specificity and sensitivity analysis performed on the phantoms [32] with embedded inclusions of varying stiffness, using a commercially available elastography system, has shown promising results.

The measurement of structural properties (stress–strain curve and hysteretic behavior) proved that phantoms have viscoelastic behavior. Preliminary results on the measurement of viscoelastic properties of the phantoms were presented in [33]. Similar work on the measurement of mechanical properties of tissues and phantoms has recently been reported [15], [34], [35]. The imaging of elastic properties of biological tissues by low-frequency harmonic vibration was presented [15], and the performance was tested using agar phantoms. The feasibility of ultrasonic shear-wave elastography in medical diagnosis [34] was demonstrated using agar-based tissue-mimicking phantoms. A handheld indentation system for assessment of mechanical properties of tissues *in vivo* was proposed [35], and the accuracy and reliability of the system were investigated using elastomers. In this paper, the viscoelastic behavior of tissue-mimicking phantoms subject to compressive loading is investigated. The storage and loss moduli of the developed phantom are also measured by adopting the same procedure as given in [3]. The normal force is recorded during this loading process and plotted. The role of models such as Maxwell, Kelvin–Voigt (KV), and Kelvin–Voigt fractional derivative (KVFD) are also investigated.

## II. THEORY

In this section, we provide a background on three models that are often used to characterize the viscoelastic behavior of biological tissues. It also includes relevant aspects of measurements. The viscoelastic behavior of biological tissues can be measured experimentally using variety of methods. The objective is to determine the relations among stress, strain, and time for a particular type of deformation and loading pattern. One of the methods is based on applying a periodic compressive displacement to a cylindrical sample of uniform thickness and cross-sectional area and measuring the force response [1], [7],

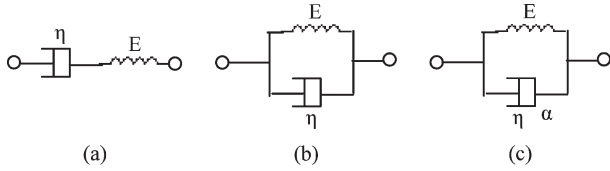


Fig. 1. Schematic representation of the (a) Maxwell, (b) KV, and (c) KVFD models.  $E$  is the elastic constant,  $\eta$  is the viscosity, and  $\alpha$  is the order of the fractional derivative.

[36]. If the viscoelastic behavior is linear, the strain will also sinusoidally alternate but will be out of phase ( $\delta$ ) with stress. The stress can vectorially be decomposed into two components, one in phase with the strain and the other  $90^\circ$  out of phase. The complex modulus is given by

$$G^* = G' + iG'' \quad (1)$$

The real part of the complex modulus  $G'$  is known as the storage modulus, as it is an indicator of the material's ability to store energy. The imaginary part  $G''$  is known as the loss modulus, which is related to the amount of energy lost through viscous processes.

The storage modulus  $G'$  and the loss modulus  $G''$  can be derived from (1) as

$$G' = |G^*| \cos \delta \quad G'' = |G^*| \sin \delta \quad (2)$$

In creep and stress relaxation experiments, the transient loading pattern is used.

#### A. Maxwell Model

The Maxwell model is represented by a purely elastic spring and a purely viscous damper connected [37] in series [Fig. 1(a)]. The model can be represented by the following equation:

$$\frac{d\varepsilon_{\text{Total}}}{dt} = \frac{d\varepsilon_D}{dt} + \frac{d\varepsilon_S}{dt} = \frac{\sigma}{\eta} + \frac{1}{E} \frac{d\sigma}{dt} \quad (3)$$

The complex modulus is given by

$$E^*(\omega) = \frac{E\eta^2\omega^2 + i\omega E^2\eta}{\omega^2\eta^2 + E^2} \quad (4)$$

Here,  $E$  is the elastic constant,  $\eta$  is the viscosity,  $\sigma$  is the stress,  $\varepsilon$  is the strain, and  $\omega$  represents the angular frequency. Suffixes  $D$  and  $S$  stand for dashpot and spring, respectively. The expression for the storage and loss moduli can be obtained from the real and imaginary parts of (4). With this model, the stresses gradually relax when the material is put under a constant strain. When a material is put under a constant stress, the strain has two components. First, an elastic component instantaneously occurs, corresponding to the spring, and immediately relaxes upon release of the stress. The second is a viscous component that grows with time as long as the stress is applied.

#### B. KV Model

The model consists of a damper and a spring connected in parallel [37] [Fig. 1(b)]. The stress is related to the strain by the equation

$$\sigma(t) = E\varepsilon(t) + \eta \frac{d\varepsilon}{dt} \quad (5)$$

The complex modulus is given by

$$E^*(\omega) = E + i\omega\eta \quad (6)$$

This model is simple but is insufficient in predicting the frequency-dependent complex modulus for viscoelastic media [6]. The KV model accounts for both storage and loss moduli, but it does not account for relaxation. Therefore, an improved model, known as the KVFD model, was considered.

#### C. KVFD Model

The KVFD model [38] is the generalization of the KV model. It consists of a spring in parallel with a fractional derivative dashpot [6], [7], as shown in Fig. 1(c). The second term of (5) is replaced with a fractional time derivative, i.e.,

$$\sigma(t) = E\varepsilon(t) + \eta D^\alpha [\varepsilon(t)] \quad (7)$$

Where the fractional derivative operator  $D^\alpha[\ ]$  is defined by

$$D^\alpha [x(t)] = \frac{1}{\Gamma(1-\alpha)} \int_0^t \frac{x(\tau)}{(t-\tau)^\alpha} d\tau \quad (8)$$

where  $\Gamma$  is the gamma function, and  $x(t)$  is an integrable harmonic function. For the KVFD model, we restrict  $0 < \alpha < 1$ . The frequency-dependent complex modulus is expressed as

$$E^*(\omega) = E + \eta(i\omega)^\alpha \quad (9)$$

Equation (7) reduces to (5) for  $\alpha = 1$ .

Equation (9) can be written as

$$E^*(\omega) = E + \eta e^{\frac{i\pi\alpha}{2}} \omega^\alpha = \left[ E + \eta \cos\left(\frac{\pi\alpha}{2}\right) \omega^\alpha \right] + j \left[ \eta \sin\left(\frac{\pi\alpha}{2}\right) \omega^\alpha \right] \quad (10)$$

From this, the equations for the storage and loss moduli can be obtained.

#### D. Normal Force and Elasticity

When certain viscoelastic samples are sheared, a force normal to the plane of the applied shear is produced. This is called the normal force or normal stress, if the correct geometrical factors are considered. The rheometer setup used for the measurement of viscoelastic properties consists of high-sensitivity load cells capable of detecting normal forces in the range of 0.01–50 N. The transducer measures the raw force, but this can be expressed as a normal force using software once the appropriate geometrical factors are used. Measuring the normal force under steady shear conditions can also be related to the amount of elasticity in a sample, and therefore, a correlation between normal forces measured under shear and elastic moduli can be made [39]. Highly elastic samples will correspondingly exhibit high normal forces.

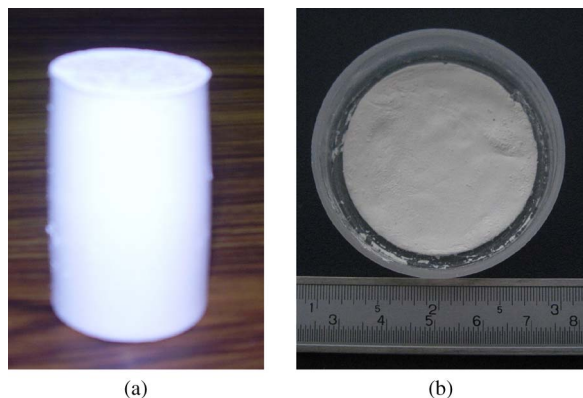


Fig. 2. Phantom for measuring (a) structural properties (diameter: 38 mm; height: 76 mm) and (b) viscoelastic properties with cyclic loading (diameter: 50 mm; height: 1.5 mm). [Phantom specifications: 0.06% initiator, 30%  $\text{TiO}_2$ , and acrylamide concentration varied from 2% to 20% in steps of 2%.]

### III. MATERIALS AND METHODS

#### A. Phantom Preparation

Acrylamide (99% pure) and  $N,N'$ -methylenebisacrylamide (99.5%) were obtained from SRL India and used as supplied. Ammonium persulfate (APS) and  $N,N,N',N'$ -tetramethylethane-1,2-diamine (TEMED) were supplied by SRL India and used without any further purification. The polymerization of acrylamide hydrogels was carried out in deionized water at room temperature (22 °C) using  $N,N'$ -methylenebisacrylamide as the cross-linker, and APS and TEMED as a pair of redox initiators. Fine particles of titanium dioxide ( $\text{TiO}_2$ ) were used to control the echogenicity of the gel. Gels of different acoustic and structural properties were prepared using different acrylamide (2%–20%) concentrations. The 40% (w/v) stock acrylamide solution was diluted in deionized water and then poured in  $\text{TiO}_2$  particles (30% w/v). The solution was degassed for 15–30 min, followed by the addition of APS and TEMED. The solution was poured into the vessels and placed in an iced water bath for about 10 min.

#### B. Measurement of the Young's Modulus and Viscoelastic Properties

Cylindrical samples with 0.06% initiator, 30%  $\text{TiO}_2$ , and varying concentration of acrylamide from 2% to 20% were prepared. The diameter of the sample was 36 mm, and the height was 76 mm [Fig. 2(a)]. The Young's modulus of the sample was measured using an unconfined compressive test setup (AIMIL Digi Tritest, AIMIL Ltd.). The samples were placed on the sample holder base, and an axial compressive load was applied on the sample with a strain rate of 0.5 mm/min until a strain of 10% was reached. The load and elongation were recorded for the prescribed loading, and the stress–strain relationship was deduced therefrom.

Thin samples with 0.06% initiator, 30%  $\text{TiO}_2$ , and varying concentration of acrylamide from 2% to 20% were prepared for measuring viscoelastic properties. The diameter of the sample was 50 mm, and the thickness was 1–2 mm [Fig. 2(b)]. The measurement of the viscoelastic properties was performed using a rheometer setup (Physica MCR 301 rheometer, M/s Anton Paar GmbH, Graz, Germany). The sample was placed in

TABLE II  
ACOUSTIC PROPERTIES OF THE PHANTOM PREPARED WITH 8% ACRYLAMIDE AND 0.06% INITIATOR. CORRESPONDING PARAMETERS FOR THE HUMAN TISSUE [40], [41] ARE ALSO GIVEN FOR COMPARISON

Parameters	Biological tissue	PAA Phantom
Velocity (m/s)	1490 – 1610 (Mean value - 1540)	1547
Attenuation (dB/MHz-cm)	0.4 – 2.0 (Mean value - 0.7)	0.44
Acoustic Impedance $\times 10^6$ (kg / m <sup>2</sup> -sec.)	1.58 – 1.70 (Mean value - 1.63)	1.67

the sample base, and parallel-plate geometry was used for the measurement. The samples were preloaded with an initial small compression level and then sequentially loaded at frequencies from 0.5 to 100 Hz. The compressor diameter was the same as that of the sample diameter to ensure uniform loading and to prevent buckling. The complex modulus  $G^*$ , storage modulus  $G'$ , and loss modulus  $G''$  were obtained using the Rheoplus software present in the system. These modulus values were fit to all the three models to determine the best-fitting model. A MATLAB curve-fitting toolbox was used for fitting the models to the experimental data using the Levenberg–Marquardt method for nonlinear least-squares fitting.

#### C. Measurement of the Normal Force

Phantoms were precompressed with a known level (5% and 20%), and then, a cyclic load with a strain rate of 5% was applied. The rheometer head initially moves down toward the sample at a preprogrammed user-defined velocity (1  $\mu\text{m/s}$ ) and reaches the specified precompression level (5% or 20%). At this point, the normal force is maximum. Then, the normal force decays to a level corresponding to the entered strain amplitude. Almost the same level of force was maintained during cyclic loading. The normal force during this phase was very small. The normal force was recorded during this entire loading process. Modulus values were also recorded during cyclic loading.

### IV. RESULTS AND DISCUSSIONS

The acoustic properties of the phantom prepared with 8% acrylamide and 0.06% initiator concentration match those of the human tissue (Table II). Here, 30%  $\text{TiO}_2$  was used to achieve the desired echogenicity [31], [32]. The stress–strain curve obtained due to loading (increasing strain) and unloading (decreasing strain) the same sample is shown in Fig. 3. The stress–strain curve is linear for stresses up to 1.8 kPa for the soft sample and up to 6 kPa for the stiff sample. The hysteresis curve shows that the sample has viscoelastic behavior and that the sample does not return to its entire unstretched length during the unloading process. Many biological soft tissues show similar behavior [1]. The large area under the hysteresis curve is due to the large stress (10 kPa), as compared with the commonly used stress (4 kPa) in biological samples [22] and other tissue-mimicking materials [26], [42].

Fig. 4 shows the measured variation in the storage and loss moduli with time, when the samples are subjected to cyclic

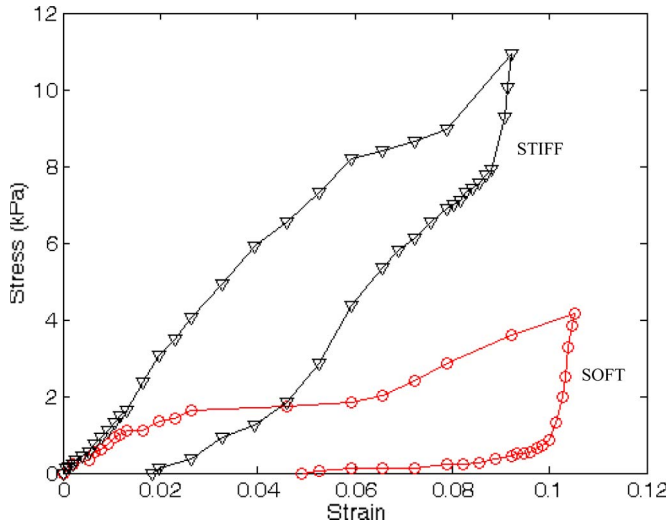


Fig. 3. Stress-strain curves for soft (6% acrylamide) and stiff (14% acrylamide) phantoms obtained during an unconfined compressive test for loading (10% strain) and unloading. [Phantom specifications: 0.06% initiator, 30% TiO<sub>2</sub>, acrylamide concentration varied from 6% to 18%, diameter 36 mm, and height 76 mm.]

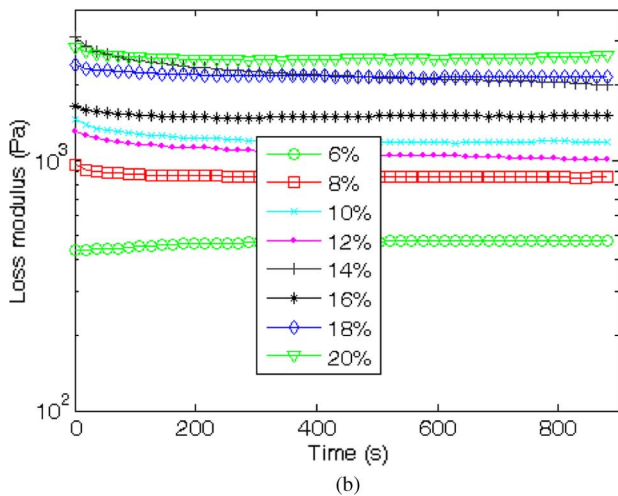
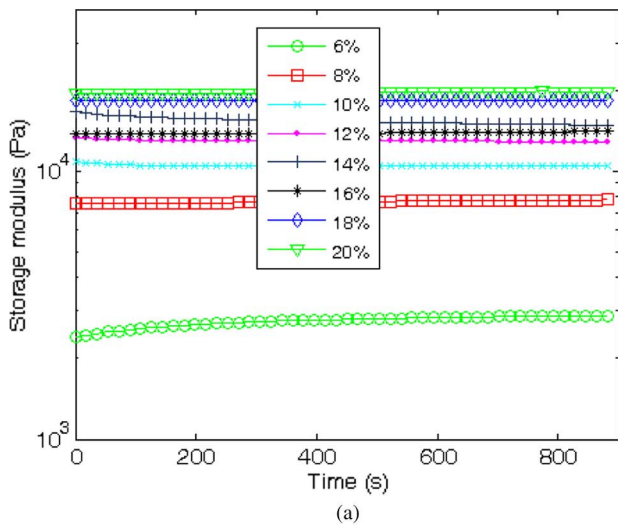


Fig. 4. Measured variations in the (a) storage modulus  $G'$  and (b) loss modulus  $G''$  with respect to time (the result of the time-sweep experiment). Sinusoidal loading is applied at a frequency of 4 Hz. [Phantom specifications: 0.06% initiator, 30% TiO<sub>2</sub>, acrylamide concentration varied from 2% to 20% in steps of 2%, diameter 50 mm, and height 1–2 mm.]

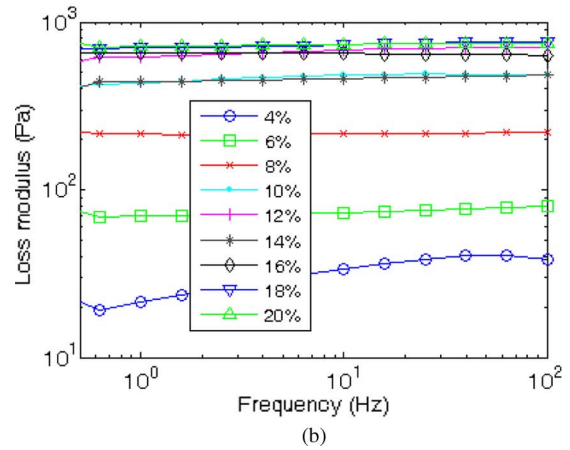
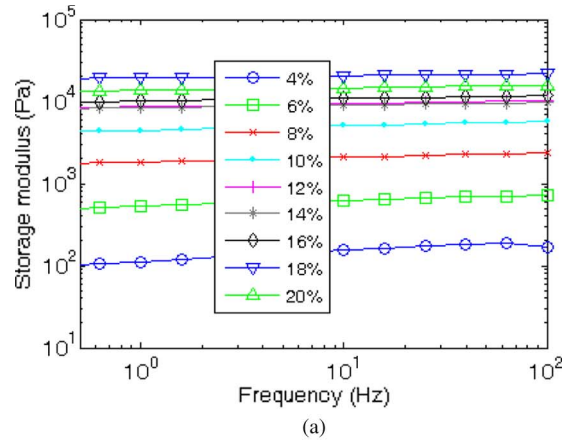


Fig. 5. Variations in the (a) storage modulus  $G'$  and (b) loss modulus  $G''$  as a function of frequency (the result of the frequency-sweep experiment) in log-log scale. Sinusoidal loading with frequencies from 0.5 to 100 Hz is applied with a compressor of diameter the same as that of the sample (50 mm). [Phantom specifications: 0.06% initiator, 30% TiO<sub>2</sub>, acrylamide concentration varied from 2% to 20% in steps of 2%, diameter 50 mm, and height 1–2 mm.]

loading at 4 Hz. There is no noticeable variation in the storage and loss moduli with time. The storage modulus is greater than the loss modulus for all monomer concentrations, which is similar to the behavior of biological tissues [3]–[8]. There is a significant increase in both moduli with the increase in monomer concentration, so that the samples cover both normal and pathological conditions. The sample with a monomer concentration of 8% represents the soft tissue and that with 20% represents the stiffer tissue. The sample with a 2% monomer concentration did not gel.

The variation of the storage and loss moduli with frequency is shown in Fig. 5. A cyclic load with frequencies of 0.5–100 Hz was applied on the cylindrical samples. The storage modulus is greater than the loss modulus for all concentrations, and the modulus values significantly increase with the increase in monomer concentration. The storage modulus values obtained by varying the monomer concentration exactly match the measured values for normal human liver [4], canine liver tissue [6], and pig kidney [8]. Both moduli slightly increase at higher frequencies. The same behavior was reported for canine liver tissue [6]. The results of fitting the models to the experimental data using the Levenberg–Marquardt method of nonlinear least-squares fitting are shown in Fig. 6. The agreement between the

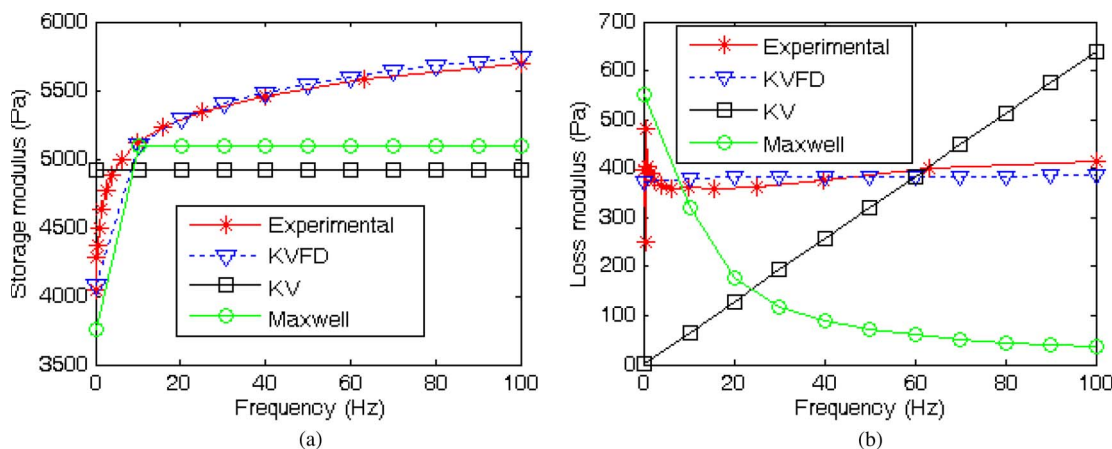


Fig. 6. Comparison of Maxwell, KV, and KVFD models. (a) Storage modulus  $G'$ . (b) Loss modulus  $G''$ . [Phantom specifications: 6% acrylamide, 0.06% initiator, and 30%  $\text{TiO}_2$ .]

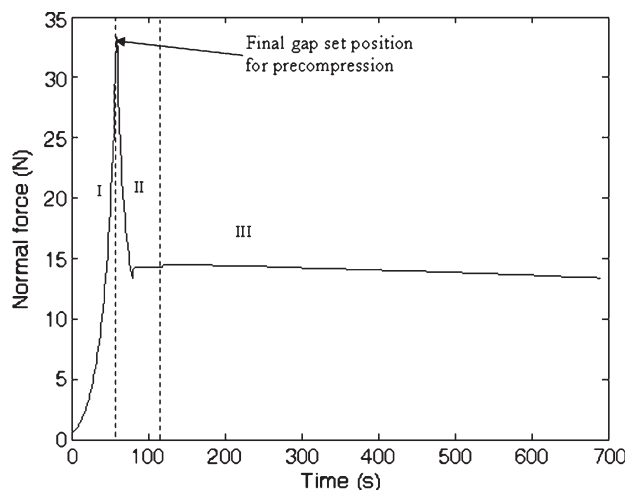


Fig. 7. Normal force during the loading process. During phase I, the sample is compressed to reach the 20% precompression level. In phase II, the normal force decays, and a small normal force exists during phase III (cyclic loading). [Phantom specifications: 18% acrylamide, 0.06% initiator, and 30%  $\text{TiO}_2$ .]

data and the model is better for the storage modulus than for the loss modulus. It is clear that the KVFD model is the only model that is close to experimental data. This is shown by the best-fit parameter  $R^2 = 0.95$ . The KV and Maxwell models are poor in representing the loss modulus.

The samples were initially precompressed to two different levels (5% and 20%), and then, a sinusoidal load with a frequency of 4 Hz is applied. Normal forces were recorded during this complete loading process. The variation of the normal force during the loading process is shown in Fig. 7. In phase I, the rheometer head moves down toward the sample at a velocity of  $1 \mu\text{m/s}$  and reaches the specified precompression level (5% or 20%). The normal force increases during this phase and reaches a maximum value when the sample is compressed to the specified level. Then, the normal force decays (phase II), and a small normal force is maintained during cyclic loading (phase III). The modulus values were also recorded during the cyclic loading phase. The variation of the normal force for samples with different monomer concentrations is shown in Fig. 8 for two precompression levels, i.e., 5% and 20%. The normal force

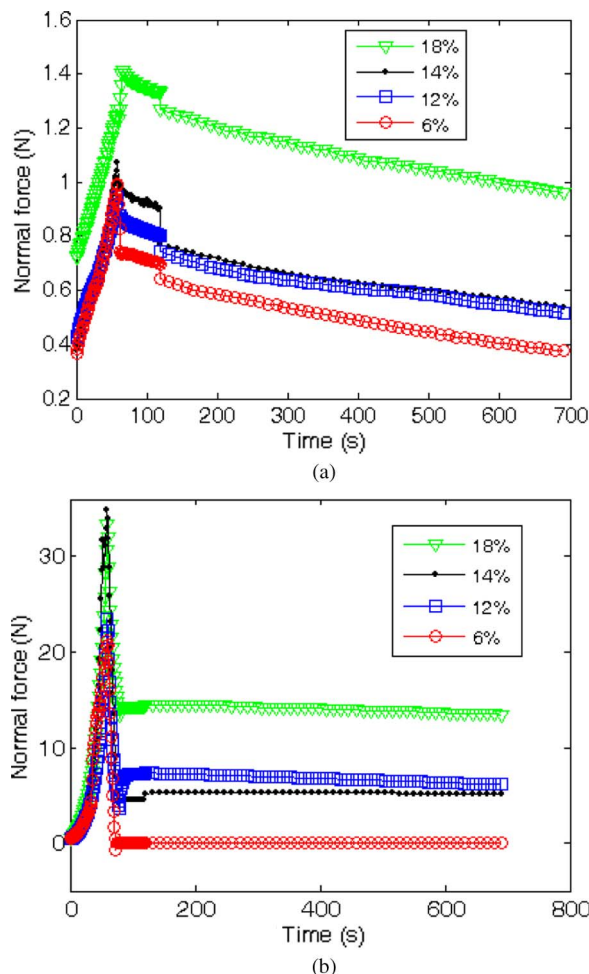


Fig. 8. Variation of the normal force with the monomer concentration during the loading process for (a) 5% and (b) 20% precompression. Results are shown for four samples with different acrylamide concentrations. [Phantom specifications: 0.06% initiator, 30%  $\text{TiO}_2$ , and acrylamide concentration varied from 2% to 20% in steps of 2%.]

during the precompression phase increases with the increase in precompression level. For a given precompression level, the normal force also increases with the increase in monomer concentration. In other words, the normal force increases with

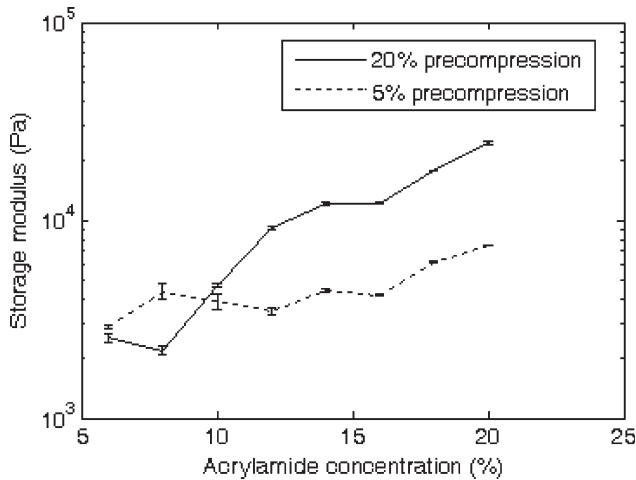


Fig. 9. Variation in the storage modulus with the monomer concentration for two different compression levels. At higher acrylamide concentrations ( $> 10\%$ ), there exists a large variation in the modulus values at two compression levels.

TABLE III  
ELASTIC MODULI (MEAN AND STANDARD DEVIATION) OF THE PHANTOMS AT TWO DIFFERENT PRECOMPRESSION LEVELS. LOADING FREQUENCY IS 4 Hz

Acrylamide concentration (%)	Elastic modulus (kPa) 5% Precompression	Elastic modulus (kPa) 20% precompression
6	$2.88 \pm 0.06$	$2.53 \pm 0.12$
8	$4.36 \pm 0.39$	$2.19 \pm 0.09$
10	$3.89 \pm 0.35$	$4.73 \pm 0.09$
12	$3.46 \pm 0.11$	$9.12 \pm 0.15$
14	$4.38 \pm 0.08$	$12.03 \pm 0.22$
16	$4.19 \pm 0.07$	$12.22 \pm 0.13$
18	$6.12 \pm 0.07$	$17.80 \pm 0.02$
20	$7.46 \pm 0.05$	$24.5 \pm 0.38$

the stiffness of the sample, justifying the fact that the normal force is a measure of sample elasticity. The highest normal force of 48 N is reached for a sample with a 20% acrylamide concentration for a 20% precompression level.

The variation in the storage modulus with the monomer concentration for two precompression levels is shown in Fig. 9. Table III presents the means and standard deviations of the elastic moduli of samples with different acrylamide concentrations at 5% and 20% precompression strain levels. At low monomer concentrations, there is no significant variation in the modulus at two compression levels. At higher monomer concentrations, there exist large variations in the modulus values at two precompression levels. Modulus values are higher (three times) at the 20% precompression level compared with 5% precompression. The same behavior was observed for breast tissues [3]. Breast cancer tissues (ductal carcinoma) are clearly differentiable from normal tissues at the 20% precompression level. The trend in variation and magnitude of the storage modulus at 5% and 20% precompression levels is exactly the same as that of a normal and pathological (fibrosis) human liver [5] at 5% and 15% precompression. This justifies the suitability of developed

TABLE IV  
COMPARISON OF THE ELASTIC MODULI OF THE DEVELOPED PHANTOMS WITH THOSE OF BIOLOGICAL TISSUES

Variation in monomer concentration	Elastic modulus	Closely matching biological tissues	comments
6% - 20%	2.8 kPa – 7.4 kPa	Pig kidney [8] Normal liver [4] Normal and cancer Breast [43]	Cyclic loading with 5% precompression
6% - 20%	2.5 kPa – 24.5 kPa	Normal and fibrosis liver [5] Normal prostate, veal liver [7]	Cyclic load with 20% precompression

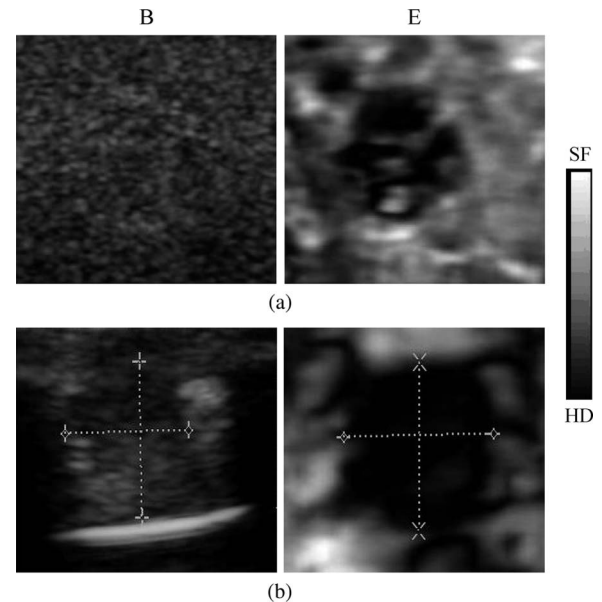


Fig. 10. Ultrasound B-mode image (B) and elastogram (E) of (a) isoechoic and (b) hyperechoic lesions. In the elastogram, black areas indicate the hard (HD) region, whereas white areas indicate the soft (SF) region. The phantom is prepared with 8% acrylamide, 30%TiO<sub>2</sub>, and 0.06% initiator. The widths of the lesions are 14 and 18 mm, respectively.

polyacrylamide phantoms for elastography applications. The comparison of the elastic moduli of the developed phantoms with those of biological tissues is presented in Table IV. The ultrasound B-mode image and elastogram of two lesions of widths 14 and 18 mm are presented in Fig. 10. The elastogram was acquired from a commercially available scanner, namely, Siemens ACUSON Antares. The lesion in Fig. 10(a) is isoechoic with different elastic moduli. This information is clearly captured in elastography. The lesion of Fig. 10(b) is hyperechoic with an irregular boundary. The lesion is clearly differentiable from the surroundings in the elastogram. This figure also shows the extent of the resolution available from elastography.

The total range of the elastic modulus achieved by varying the acrylamide concentration from 2% to 20% is 2–24 kPa. The change in modulus from the sample-mimicking normal tissue to the sample-mimicking cancerous tissue is large enough to achieve the desired contrast between the lesion and the surroundings. In ultrasound elastography applications, the difference in elastic modulus between the lesion and the surroundings is more important than the absolute value of the modulus for better lesion delineation and diagnosis.

## V. CONCLUSION

Tissue-mimicking phantoms catering to normal and pathological biological tissues have been developed. The phantoms were constructed using acrylamide as the monomer and  $\text{TiO}_2$  as the scattering medium. The measurement of structural properties of the phantoms confirmed that they exhibit viscoelastic behavior, as shown by some biological tissues. Modulus values were also measured by precompressing the sample at two different compression levels, followed by the application of a cyclic load. A large variation in the elastic modulus exists for two precompression strain levels at higher monomer concentrations. This validates the mechanical similitude of the developed phantoms with that of biological tissues. A large variation in the normal force was observed during precompression with the increase in monomer concentration. A large contrast in the elastic modulus corresponding to the tumor and the normal tissue can be achieved by suitable selection of the monomer concentration. These results can be used to provide a recipe for the preparation of phantoms for ultrasound elastography and viscoelastic imaging. Three models were explored to fit the experimental results. The results show that KVFD is the only model that describes the experimental results.

## ACKNOWLEDGMENT

The authors would like to thank Dr. A. Deshpande and G. Rakesh, Department of Chemical Engineering, IIT Madras, for providing the facility and for help in doing the measurement, as well as Prof. V. Jagadeesh Kumar for helpful discussions and suggestions.

## REFERENCES

- [1] Y. C. Fung, *Biomechanics Mechanical Properties of Living Tissues*, 2nd ed. New York: Springer-Verlag, 1993, ch. 7.
- [2] H. Yamada, *Strength of Biological Materials*. Baltimore, MD: Williams & Wilkins, 1970.
- [3] T. A. Krouskop, T. M. Wheeler, F. Kallel, B. S. Garra, and T. J. Hall, "Elastic moduli of breast and prostate tissues under compression," *Ultrason. Imag.*, vol. 20, no. 4, pp. 260–274, Oct. 1998.
- [4] Z. Liu and L. Bilston, "On the viscoelastic character of liver tissue: experiments and modeling of the linear behaviour," *Biorheology*, vol. 37, no. 3, pp. 191–201, 2000.
- [5] W. C. Yeh, Y. M. Jeng, H. C. Hsu, P. L. Kuo, M. L. Li, P. M. Yang, P. H. Lee, and P. C. Li, "Young's modulus measurement of human liver and correlation with pathological findings," in *Proc. IEEE Ultrason. Symp.*, Atlanta, GA, Oct. 7–10, 2001, pp. 1233–1236.
- [6] M. Z. Kiss and T. Varghese, "Viscoelastic characterization of *in-vitro* canine liver tissue," in *Proc. IEEE Int. Ultrason., Ferroelectr. Freq. Control Joint 50th Anniv. Conf.*, 2006, pp. 2086–2089.
- [7] M. Zhang, B. Castaneda, Z. Wu, N. Priya, J. V. Joseph, D. J. Rubens, and K. J. Parker, "Congruence of imaging estimators and mechanical measurements of viscoelastic properties of soft tissues," *Ultrasound Med. Biol.*, vol. 33, no. 10, pp. 1617–1631, Oct. 2007.
- [8] S. Nasser, L. E. Bilston, and N. Phan-Thein, "Viscoelastic properties of pig kidney in shear, experimental results and modeling," *Rheol. Acta*, vol. 41, no. 1/2, pp. 180–192, Jan. 2002.
- [9] D. P. Noonan, H. Liu, Y. H. Zweiri, K. A. Althoefer, and L. D. Seneviratne, "A dual-function wheeled probe for tissue viscoelastic property identification during minimally invasive surgery," in *Proc. IEEE Int. Conf. Robot. Autom.*, Roma, Italy, Apr. 10–14, 2007, pp. 2629–2634.
- [10] H. Liu, D. P. Noonan, K. A. Althoefer, and L. D. Seneviratne, "Rolling mechanical imaging: A novel approach for soft tissue modeling and identification during minimally invasive surgery," in *Proc. IEEE Int. Conf. Robot. Autom.*, Pasadena, CA, May 19–23, 2008, pp. 845–850.
- [11] J. Ophir, I. Cespedes, H. Ponnekanti, Y. Yazdi, and X. Li, "Elastography: A quantitative method for imaging the elasticity of biological tissues," *Ultrason. Imag.*, vol. 13, no. 2, pp. 111–134, Apr. 1991.
- [12] B. S. Garra, E. I. Cespedes, J. Ophir, S. R. Spratt, R. A. Zurbier, C. M. Magnant, and M. F. Pennanen, "Elastography of breast lesions: Initial clinical results," *Radiology*, vol. 202, no. 1, pp. 79–86, Jan. 1997.
- [13] A. Lyshchik, T. Higashi, R. Asato, S. Tanaka, J. Ito, J. J. Mai, C. Pellet-Barakat, M. F. Insana, A. B. Brill, T. Saga, M. Hiroaka, and K. Togashi, "Thyroid gland tumor diagnosis at US elastography," *Radiology*, vol. 237, no. 1, pp. 202–211, Oct. 2005.
- [14] A. Manduca, T. E. Oliphant, M. A. Dresner, J. L. Mahowald, S. A. Kruse, E. Amromin, J. P. Felmlee, J. F. Greenleaf, and R. L. Ehman, "Magnetic resonance elastography: Non-invasive mapping of tissue elasticity," *Med. Image Anal.*, vol. 5, no. 4, pp. 237–254, Dec. 2001.
- [15] M. Fatemi, A. Manduca, and J. F. Greenleaf, "Imaging of elastic properties of biological tissues by low-frequency harmonic vibration," *Proc. IEEE*, vol. 91, no. 10, pp. 1503–1519, Oct. 2003.
- [16] J. Ophir, S. K. Alam, B. Garra, F. Kallel, E. Konofagou, and T. Varghese, "Elastography: Ultrasonic estimation and imaging of the elastic properties of tissues," in *Proc. Inst. Mech. Eng. H*, 1999, vol. 213, no. 3, pp. 203–233.
- [17] L. S. Taylor, M. S. Richards, A. J. Moskowitz, A. L. Lerner, D. J. Rubens, and K. J. Parker, "Viscoelastic effects in sonoelastography: Impact on tumor detectability," in *Proc. IEEE Ultrason. Symp.*, Atlanta, GA, Oct. 7–10, 2001, pp. 1639–1642.
- [18] W. F. Walker, F. J. Fernandes, and L. A. Negron, "A method of imaging viscoelastic parameters with acoustic radiation force," *Phys. Med. Biol.*, vol. 45, no. 6, pp. 1437–1447, Jun. 2000.
- [19] M. Fatemi and J. E. Greenleaf, "Probing the dynamics of tissue at low frequencies with the radiation force of ultrasound," *Phys. Med. Biol.*, vol. 45, no. 6, pp. 1449–1464, Jun. 2000.
- [20] A. Itoh, E. Ueno, E. Tohno, H. Kamma, H. Takahashi, T. Shiina, M. Yamakawa, and T. Matsumura, "Breast disease: Clinical application of US elastography for diagnosis," *Radiology*, vol. 239, no. 4, pp. 341–350, 2006.
- [21] T. Rago, F. Santini, M. Scutari, A. Pinchera, and P. Vitti, "Elastography: New developments in ultrasound for predicting malignancy in thyroid nodules," *J. Clin. Endocrinol. Metab.*, vol. 92, no. 8, pp. 2917–2922, Aug. 2007.
- [22] M. Sridhar, "Imaging viscoelasticity in hydropolymers and breast tissue with ultrasound," Ph.D. dissertation, Univ. California, Davis, Davis, CA, 2006.
- [23] A. Eder, T. Arnold, and C. Kargel, "Performance evaluation of displacement estimators for real-time ultrasonic strain and blood flow imaging with improved spatial resolution," *IEEE Trans. Instrum. Meas.*, vol. 56, no. 4, pp. 1275–1284, Aug. 2007.
- [24] C. Kargel, G. Pelvnik, B. Trummer, and M. F. Insana, "Doppler ultrasound systems designed for blood flow imaging," *IEEE Trans. Instrum. Meas.*, vol. 53, no. 2, pp. 524–536, Apr. 2004.
- [25] J. Wu, G. Wang, D. Ye, and Y. Wang, "A new system for soft-tissue balance measurement in total knee replacement," *IEEE Trans. Instrum. Meas.*, vol. 58, no. 10, pp. 3627–3632, 2009.
- [26] M. Sridhar, J. Liu, and M. F. Insana, "Elasticity imaging of polymeric media," *Trans. ASME, J. Biomech. Eng.*, vol. 129, no. 2, pp. 259–272, 2007.
- [27] C. U. Devi, R. S. B. Chandran, R. M. Vasu, and A. K. Sood, "Measurement of visco-elastic properties of breast-tissue mimicking materials using diffusing wave spectroscopy," *J. Biomed. Opt.*, vol. 12, no. 3, pp. 034 035–1–034 035–5, May/Jun. 2007.
- [28] L. A. Negron, F. Viola, E. P. Black, C. A. Toth, and W. F. Walker, "Development and characterization of vitreous mimicking material for radiation force imaging," *IEEE Trans. Ultrason., Ferroelectr., Freq. Control*, vol. 49, no. 11, pp. 1543–1551, Nov. 2002.
- [29] K.-I. Kawabata, Y. Waki, T. Matsumura, and S.-I. Umemura, "Tissue mimicking phantom for ultrasonic elastography with finely adjustable elastic and echographic properties," in *Proc. IEEE Ultrason., Ferroelectr. Freq. Control Joint 50th Anniv. Conf.*, 2004, pp. 1502–1505.
- [30] K. Kumar, V. Jayashankar, S. Suresh, M. E. Andrews, and A. K. Mishra, "Image processing based characterization of tissue phantoms for ultrasound elastography applications," in *Proc. Int. Conf. Comput. Commun. Control Instrum.*, Bangalore, India, 2007, pp. 396–399.
- [31] K. Kumar, M. E. Andrews, V. Jayashankar, A. K. Mishra, and S. Suresh, "Design development and characterization of cyst phantoms for ultrasound elastography applications," in *Proc. 30th Annu. Int. IEEE EMBS Conf.*, Vancouver, BC, Canada, Aug. 20–24, 2008, pp. 2872–2975.

- [32] K. Kumar, V. Jayashankar, S. Suresh, M. E. Andrews, and A. K. Mishra, "Improved diagnosis of breast tumor by combining ultrasound B mode and elastography-phantom based analysis," in *Proc. Int. Conf. Biomed. Eng.*, Kuala Lumpur, Malaysia, Jun. 25–28, 2008, pp. 579–582.
- [33] K. Kumar, V. Jayashankar, V. J. Kumar, M. E. Andrews, and A. K. Mishra, "Viscoelastic properties of tissue mimicking phantoms for ultrasound elastography applications," in *Proc. I2MTC*, May 4–7, 2009, pp. 1510–1513.
- [34] V. Rengaraju, A. F. F. da Silva, I. Sack, and C. Kargel, "A basic study of ultrasound shear wave elastography in tissue-mimicking phantoms," in *Proc. IEEE Int. Workshop Med. Meas. Appl.*, Cetraro, Italy, May 29–30, 2009, pp. 55–59.
- [35] M.-H. Lu, W. Yu, Q.-H. Huang, Y.-P. Huang, and Y.-P. Zheng, "A hand held indentation system for the assessment of mechanical properties of soft tissue in vivo," *IEEE Trans. Instrum. Meas.*, vol. 58, no. 9, pp. 3079–3085, Sep. 2009.
- [36] J. D. Ferry, *Viscoelastic Properties of Polymers*. Hoboken, NJ: Wiley, 1961, ch. 5/6.
- [37] M. A. Meyers and K. K. Chawla, *Mechanical Behavior of Materials*. Englewood Cliffs, NJ: Prentice-Hall, 1999.
- [38] R. L. Bagley, "A theoretical basis for the application of fractional calculus to viscoelasticity," *J. Rheol.*, vol. 27, no. 3, pp. 201–210, Jun. 1983.
- [39] H. A. Barnes, J. F. Hutton, and K. Walters, *An Introduction to Rheology*. Amsterdam, The Netherlands: Elsevier, 1989.
- [40] G. D. Ludwig, "The velocity of sound through tissues and the acoustic impedance of tissues," *J. Acoust. Soc. Amer.*, vol. 22, no. 6, pp. 862–866, Nov. 1950.
- [41] C. R. Hill, J. C. Bamber, and G. R. ter Haar, *Physical Principles of Medical Ultrasonics*. Hoboken, NJ: Wiley, 2004, pp. 217–219.
- [42] T. J. Hall, M. Bilgen, M. F. Insana, and T. A. Krouskop, "Phantom materials for elastography," *IEEE Trans. Ultrason., Ferroelectr., Freq. Control*, vol. 44, no. 6, pp. 1355–1365, Nov. 1997.
- [43] J. Bercoff, M. Tanter, and M. Fink, "Supersonic shear imaging: A new technique for soft tissue elasticity mapping," *IEEE Trans. Ultrason., Ferroelectr., Freq. Control*, vol. 51, no. 4, pp. 396–709, Apr. 2004.



**Kishore Kumar** (S'09) was born in Bantwala, India, on April 3, 1979. He received the B.E. degree in instrumentation technology from the University of Mysore, Mysore, India, in 2001 and the M.Tech. degree in biomedical signal processing and instrumentation from Visvesvaraya Technological University, Belgaum, India, in 2004. He is currently working towards the Ph.D. degree in biomedical instrumentation with the Department of Electrical Engineering, Indian Institute of Technology Madras, Chennai, India.

His interests are in the areas of biomedical instrumentation, medical imaging, ultrasound elastography, and human vision.



**Maneesha E. Andrews** was born in Gorakhpur, India, on September 10, 1973. She received the B.Sc. and M.Sc. degrees in chemistry from Agra University, Agra, India, in 1994 and 1996, respectively, and the Ph.D. degree in chemistry from the University of Madras, Chennai, India, in 2006.

She is currently a Postdoctoral Fellow with the Department of Chemistry, Indian Institute of Technology Madras, Chennai. Her areas of interest are peptide and polymer chemistry, spectroscopy, and quantum chemical calculations.

**V. Jayashankar** (M'05) received the B.Tech. degree from Banaras Hindu University, Varanasi, India, in 1982, the M.S. degree from Indian Institute of Technology (IIT) Madras, Chennai, India, in 1991, and the Ph.D. degree from the College of Engineering, Guindy, Chennai, in 1994, all in electrical engineering.

From 1994 to 2000, he was with the National Institute of Ocean Technology, Chennai. He is currently a Professor with the Department of Electrical Engineering, IIT Madras.



**Ashok K. Mishra** was born in Titlagarh, India, on March 10, 1959. He received the M.Sc. degree from Delhi University, New Delhi, India, in 1980 and the Ph.D. degree from Indian Institute of Technology (IIT), Kanpur, India, in 1985.

He was a Monbusho Fellow during 1987–1989 and a JSPS Visiting Scientist during 2002–2003 with Gunma University, Maebashi, Japan. He is currently a Professor with the Department of Chemistry, IIT Madras, Chennai, India. He has published more than 100 papers in international journals. His teaching and research interests are in physical photochemistry and fluorescence spectroscopy.

Prof. Mishra is a Fellow of the National Academy of Sciences, India.



**S. Suresh** was born in Chennai, India, on October 28, 1953. He received the M.B.B.S. degree from Chengalpattu Medical College, Chengalpattu, India, in 1976.

He underwent ultrasound training at Sir H. N. Hospital, Bombay, India, in 1982 and advanced training in abdomen/pelvis and Doppler ultrasound at Thomas Jefferson University, Philadelphia, PA, and John's Hopkins University, Baltimore, MD, in 1984. He is certified as a Registered Diagnostic Medical Sonographer by the American Registry of Diagnostic

Medical Sonographers in 1994. He is currently the Director of Mediscan Systems, Chennai. He has published several papers and articles in national and international Journals. His interests are in the areas of fetal therapy and interventions, as well as ultrasound elastography.